Journal of Alloys and Compounds 514 (2012) 199–204

Contents lists available at SciVerse ScienceDirect

Journal of Alloys and Compounds

journal homepage: www.elsevier.com/locate/jallcom

X-ray photoelectron and absorption spectroscopy of mixed lanthanum copper oxychalcogenides $LaCuOSe_{1-x}Te_x$ $(0 \leq x \leq 1)$

Brent W. Rudyk, Peter E.R. Blanchard, Ronald G. Cavell, Arthur Mar*

Department of Chemistry, University of Alberta, Edmonton, Alberta, Canada T6G 2G2

ARTICLE INFO

Article history:
Received 22 August 2011
Received in revised form 8 November 2011
Accepted 13 November 2011
Available online 20 November 2011

Keywords:
Oxychalcogenides
Solid solution
XPS
XANES
Charge potential model

ABSTRACT

The complete oxychalcogenide solid solution $LaCuOSe_{1-x}Te_x$ $(0 \leq x \leq 1)$ was examined by X-ray photoelectron and X-ray absorption near-edge spectroscopy. Whereas the La 3d, Cu 2p and most of the chalcogen (*Ch*) core-line peaks are invariant, the O 1s binding energies (BE) show shifts (up to 0.35 eV) with increasing substitution of Se by Te that reflect the competing effects of the charges of neighbouring La atoms and more distant *Ch* atoms, if the charge potential model is applied. This observation supports the occurrence of interlayer La–*Ch* interactions between the [LaO] and [Cu*Ch*] layers in LaCuO*Ch*. The Se 3d BEs show smaller shifts (up to 0.15 eV) that indicate the development of more negative charge on the Se atoms with increasing *x*. The Cu K-edge and Se K-edge spectra reveal subtle absorption edge energy and intensity changes that can be explained by the evolution of Cu-to-*Ch* charge transfer within the [Cu*Ch*] layers.

1. Introduction

The quaternary rare-earth copper oxychalcogenides *RE*CuO*Ch* (*Ch* = S, Se, Te) have been explored for potential applications in optoelectronic devices as transparent p-type semiconductors [1–7]. They belong to the large family of tetragonal ZrCuSiAs-type materials [8,9], which include the rare-earth transition-metal oxypnictides *REMPn*O (*P* = P, As), now in vogue owing to their high-temperature superconducting behaviour [10–14]. The interesting physical properties exhibited by these compounds depend on the complex interplay of electronic interactions between the covalent, conducting [Cu*Ch*] or [*MPn*] layers and the ionic, insulating [*RE*O] layers which are alternately stacked along the *c*-direction in their tetragonal structures (inset of Fig. 1). Evaluating the degree of charge transfer within and between these layers is important for understanding how these properties can be modified. Previous analyses of X-ray photoelectron (XPS) and X-ray absorption near-edge spectra (XANES) support the picture of a highly two-dimensional layered structure for *RE*CuO*Ch* and *REMPn*O [15–17], in contrast to tetrelide pnictides like ZrCuSiAs itself, which shows three-dimensional bonding character [18,19]. However, in the LaCuO*Ch* (*Ch* = S, Se, Te) series, there is evidence for the occurrence of weak interlayer La–*Ch* interactions between the [LaO] and [Cu*Ch*] layers that become enhanced with larger *Ch* atoms, through the observation of changes in the intensity of a satellite feature in the La 3d XPS spectra [17]. Intralayer Cu–*Ch* interactions would also be expected within the [Cu*Ch*] layers, but these were more problematic to detect because of final-state effects in the Cu 2p XPS spectra.

The mixed-chalcogenide solid solution $LaCuOSe_{1-x}Te_x$ $(0 \leq x \leq 1)$ presents an attractive opportunity to analyze these electronic interactions in more detail. Here, we report firmer evidence for interlayer interactions between the [LaO] and [Cu*Ch*] layers, as manifested by shifts in binding energies (BEs) in the O and *Ch* XPS spectra that are influenced by the chemical environment. We also probe the nature of the intralayer Cu–*Ch* interactions within the [Cu*Ch*] layers by examining changes in the Cu K-edge and Se K-edge XANES spectra, which are less sensitive to final-state effects.

2. Experimental

2.1. Synthesis

Reagents in the form of pieces (La) or powders (La_2O_3, Cu, Se, and Te) with purities of 99.5% or better were obtained from Cerac, Aldrich, or Alfa-Aesar. La_2Se_3 was obtained by stoichiometric reaction of La and Se at 900 °C for 1 week.

LaCuOSe was prepared by heating a mixture of La_2O_3, La_2Se_3, Cu, and Se in a 2:1:6:3 ratio in an evacuated and sealed fused-silica tube at 1050 °C for 10 days. LaCuOTe was prepared by heating a mixture of La, La_2O_3, Cu, and Te in a 1:1:3:3 ratio in an evacuated and sealed fused-silica tube at 1050 °C for 1–2 weeks; regrinding the quenched product and reheating for an additional week was required for complete reaction. Members of the solid solution $LaCuOSe_{1-x}Te_x$ (x = 0.2, 0.3, 0.4, 0.6, 0.8) were prepared by heating mixtures of the end-members LaCuOSe and LaCuOTe in appropriate ratios at 1050 °C in three cycles of 4 days each, with intermediate grindings. All compounds were found to be >98% pure, as determined by comparing the intensities of the strongest peaks relative to those for impurity phases in their powder

* Corresponding author. Fax: +1 780 492 8231.
E-mail address: arthur.mar@ualberta.ca (A. Mar).

0925-8388/$ – see front matter © 2011 Elsevier B.V. All rights reserved.
doi:10.1016/j.jallcom.2011.11.063

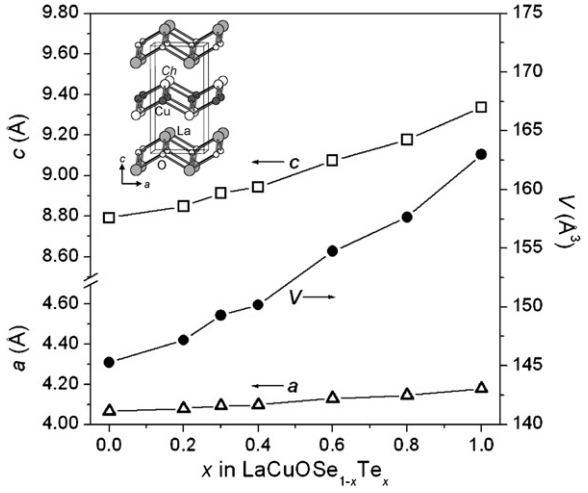

Fig. 1. Plot of cell parameters vs. x for $LaCuOSe_{1-x}Te_x$ forming the tetragonal ZrCuSiAs-type structure (inset). The lines are shown only to guide the eye.

Table 1
Cell parameters for $LaCuOSe_{1-x}Te_x$.

Compound	a (Å)	c (Å)	V (Å^3)
LaCuOSe	4.0651(1)	8.7914(2)	145.28(1)
$LaCuOSe_{0.8}Te_{0.2}$	4.0784(1)	8.8485(3)	147.18(1)
$LaCuOSe_{0.7}Te_{0.3}$	4.0927(1)	8.9128(2)	149.29(1)
$LaCuOSe_{0.6}Te_{0.4}$	4.0976(1)	8.9434(3)	150.16(1)
$LaCuOSe_{0.4}Te_{0.6}$	4.1294(1)	9.0748(2)	154.74(1)
$LaCuOSe_{0.2}Te_{0.8}$	4.1447(1)	9.1768(2)	157.64(1)
LaCuOTe	4.1783(1)	9.3363(3)	163.00(1)

X-ray diffraction (XRD) patterns (Fig. S1 in Supplementary Data) collected on an Inel diffractometer equipped with a CPS 120 detector. The cell parameters (Table 1) for this complete solid solution increase regularly as x increases in $LaCuOSe_{1-x}Te_x$, consistent with the substitution of larger Te for Se atoms (Fig. 1). The cell volume exhibits a small negative deviation from a strictly linear Vegard's law dependence, suggesting that there may be slight local ordering of the chalcogen atoms when the concentrations of Se and Te are similar. A similar behaviour was previously observed for the $LaCuOS_{1-x}Se_x$ solid solution [20].

2.2. XPS analysis

XPS spectra were measured on a Kratos AXIS 165 spectrometer equipped with a monochromatic Al Kα X-ray source (15 kV, 14 mA) and a hybrid lens with a spot size of 700 μm × 400 μm. The air-stable samples were finely ground, pressed onto In foil, mounted on a Cu sample stage with carbon tape, and transferred to the spectrometer chamber in which the pressure was maintained between 10^{-7} and 10^{-9} Pa. The samples were sputter-cleaned with an Ar^+ beam (4 kV, 10 mA) to remove surface oxides as much as possible until no further changes were observed in the survey spectra. No visible chemical reduction occurred as a result of this sputtering procedure. Charge neutralization was attempted but was concluded to be unnecessary.

Survey spectra (collected with a BE range of 0–1100 eV, a pass energy of 160 eV, a step size of 0.7 eV, and a sweep time of 180 s) confirmed the presence of all elements in the expected compositions. High-resolution La 3d, Cu 2p, O 1s, Se 3p, Se 3d, Te 3d, and Te 4d core-line spectra (collected with a BE range appropriate for each element as determined from the survey spectra, a pass energy of 20 eV, a step size of 0.05 eV, and a sweep time of 180 s) were calibrated to the C 1s line at 284.8 eV arising from adventitious carbon. These spectra were analyzed with use of the CasaXPS software package [21]. The background arising from energy loss was removed by applying a Shirley-type function and the peaks were fitted to pseudo-Voigt (70% Gaussian and 30% Lorentzian) line profiles to take into account spectrometer and lifetime broadening effects. Table 2 lists the observed BE values, with uncertainties estimated to be better than ±0.1 eV obtained from singly measured spectra, on the basis of previous measurements on this instrument. Because small shifts in the O 1s and Se 3d BEs were noted, these spectra were re-collected for all members of the solid solution (including the previously measured end-members LaCuOSe and LaCuOTe [17]) to obtain more precise values. For each member, two or three samples from the same synthesis batch were separately ground, sputter-cleaned, and examined individually (Table S1 in Supplementary Data). On the basis of these multiply measured spectra, the O 1s and Se 3d BEs were averaged and expressed to two decimal places in Table 2. Their uncertainties evaluated from $(ts)/\sqrt{n}$, where t values were taken at a 95% confidence interval, s is the standard deviation, and n is the number of measurements, were generally better than ±0.05 eV.

2.3. Cu K- and Se K-edge XANES analyses

Cu K- and Se K-edge XANES spectra were measured on the bending magnet beamline (20 BM) at the Advanced Photon Source (APS) accessed through the Pacific Northwest Consortium/X-ray Operations and Research Collaborative Access Team (PNC/XOR-CAT), Sector 20, at Argonne National Laboratory. Finely ground samples were sandwiched between Kapton tape and positioned at 45° to the X-ray beam, which has a resolution of 1.4 eV at 10 keV, a spot size of 1 mm × 4.5 mm, and a photon flux of ~10^{11} photons/s provided by a silicon (1 1 1) double crystal monochromator. Spectra were collected in both transmission mode (through an ionization detector filled with a 60:40 mixture of He and N_2) and fluorescence mode (through a 4-element Vortex detector for the Cu K-edge and a 13-element Canberra detector for the Se K-edge). The step size through the absorption edge was 0.25 eV. Standards of elemental Cu and Se were placed behind the sample and measured simultaneously, with the maxima in the first derivatives set to 8979 eV for the Cu K-edge and 12,658 eV for the Se K-edge. Calibration values were obtained from the program Hephaestus and the spectra were analyzed with the program Athena, both in the Ifeffit software package [22]. Uncertainties in the absorption energies are estimated to be better than ±0.1 eV on the basis of multiple scans. All observed absorption edge energies are listed in Table 2.

2.4. Band structure calculations

The interpretation of XANES spectra was facilitated by evaluating the character of empty conduction states in LaCuOSe and LaCuOTe determined by tight-binding linear muffin tin orbital (TB-LMTO) band structure calculations performed within the local density and atomic spheres approximation with use of the Stuttgart

Table 2
XPS binding energies (eV) and XANES absorption edge energies (eV) for members of the solid solution $LaCuOSe_{1-x}Te_x$.

Compound	LaCuOSe	$LaCuOSe_{0.8}Te_{0.2}$	$LaCuOSe_{0.7}Te_{0.3}$	$LaCuOSe_{0.6}Te_{0.4}$	$LaCuOSe_{0.4}Te_{0.6}$	$LaCuOSe_{0.2}Te_{0.8}$	LaCuOTe[a]
La $3d_{5/2}$	834.3(1)[a]	834.4(1)	834.4(1)	834.5(1)	834.4(1)	834.4(1)	834.5(1)[a]
La $3d_{3/2}$	851.1(1)[a]	851.2(1)	851.2(1)	851.4(1)	851.3(1)	851.2(1)	851.2(1)[a]
Cu $2p_{3/2}$	932.8(1)[a]	932.8(1)	932.9(1)	932.9(1)	932.8(1)	932.9(1)	932.9(1)[a]
Cu $2p_{1/2}$	952.6(1)[a]	952.6(1)	952.7(1)	952.8(1)	952.6(1)	952.7(1)	952.7(1)[a]
Cu K-edge[b]	8986.1(1)	8986.0(1)	8985.8(1)	8985.8(1)	8985.7(1)	8985.6(1)	8985.3(1)
O 1s[c]	529.77(5)	529.63(5)	529.61(10)	529.58(2)	529.51(5)	529.42(5)	529.74(3)
Se $3d_{5/2}$[c]	53.93(3)	53.86(3)	53.85(3)	53.85(3)	53.83(3)	53.78(3)	
Se $3d_{3/2}$[c]	53.78(3)	54.71(3)	54.70(3)	54.70(3)	54.68(3)	54.63(3)	
Se $3p_{3/2}$	160.1(1)[a]	160.2(1)	160.2(1)	160.2(1)	160.1(1)	160.3(1)	
Se $3p_{1/2}$	165.9(1)[a]	166.0(1)	166.0(1)	166.0(1)	165.8(1)	165.9(1)	
Se L-edge	1429.6(1)	1429.4(1)	1429.4(1)	1429.5(1)	1429.5(1)	1429.4(1)	
Se K-edge	12658.2(1)	12658.3(1)	12658.3(1)	12658.3(1)	12658.3(1)	12658.4(1)	
Te $4d_{5/2}$		40.2(1)	40.3(1)	40.3(1)	40.2(1)	40.2(1)	40.2(1)[a]
Te $4d_{3/2}$		41.7(1)	41.7(1)	41.7(1)	41.6(1)	41.6(1)	41.7(1)[a]
Te $3d_{5/2}$		572.7(1)	572.7(1)	572.7(1)	572.6(1)	572.6(1)	572.6(1)[a]
Te $3d_{3/2}$		583.1(1)	583.1(1)	583.1(1)	583.0(1)	583.0(1)	582.9(1)[a]

[a] Taken from Ref. [17].
[b] Cu K-pre-edge located at 8980.6(1) eV for all samples.
[c] O 1s and Se 3d BEs were averaged from multiply measured spectra, with uncertainties quoted at a 95% confidence interval.

TB-LMTO-ASA program (version 4.7) [23]. Integrations were carried out over 84 independent *k* points within the first Brillouin zone.

3. Results and discussion

3.1. XPS spectra

An initial examination of the core-line XPS spectra for the solid solution $LaCuOSe_{1-x}Te_x$ ($0 \le x \le 1$) revealed no prominent differences. Although the *Ch* atoms are closest to the La and Cu atoms, the gradual substitution of Se with Te is not reflected in any visible changes in the La 3d and Cu 2p spectra, which are strongly influenced by final state effects (Fig. S2 in Supplementary Data) [24–29]. The La 3d spectra contain a satellite peak which was previously attributed to a ligand-to-metal shake-up process and which serves to measure the degree of orbital overlap between La and *Ch* atoms [17,27–29], but the differences are too small between the end-members LaCuOSe and LaCuOTe for this feature to be helpful to monitor. Similarly, the Cu 2p spectra are invariant, and in any case, the Cu $2p_{3/2}$ BE cannot be probed reliably to obtain information about oxidation state [30,31]. Final state effects are quite prominent in Cu XPS spectra, as has been noted previously [32]. When a core-hole is generated upon photoionization, interatomic relaxation can take place whereby electron density from surrounding atoms flows towards it, enhancing the screening so that the final state energy is decreased and the BE is apparently lowered. This relaxation becomes more pronounced with higher oxidation state of the Cu atom, and it becomes difficult to separate ground-state from final-state effects in Cu XPS spectra [32].

Each of the O 1s XPS spectra reveals a main core-line peak inherent to the oxychalcogenide at lower BE and a second peak attributed to surface oxides that is typically found at higher BE (Fig. 2a) [15,16]. Although surface oxides are normally difficult to eliminate entirely, they were minimized through sputter-cleaning for a duration that does not risk damaging the sample. In the course of this sputtering procedure, the intensity of the peak arising from surface oxides diminished while the position of the main core-line peak for the oxychalcogenide remained invariant. Surprisingly, we noted subtle changes in the O 1s XPS spectra in which there were small BE shifts of up to ~0.2 eV, just above the limits of uncertainty (±0.1 eV). These spectra were recollected multiple times to improve statistics, confirming a real trend in the O 1s BEs (Table 2 and Fig. 2a). As Se is substituted with Te, the O 1s BE gradually decreases from 529.77(2) eV in LaCuOSe to 529.42(2) eV in $LaCuOSe_{0.2}Te_{0.8}$, but then it abruptly returns to 529.74(1) eV in LaCuOTe. Differences in the *Ch* XPS spectra were more difficult to detect. Multiply measured Se 3d spectra suggest a gradual decrease in the Se $3d_{5/2}$ BE from 53.93(1) eV in LaCuOSe to 53.78(1) eV in $LaCuOSe_{0.2}Te_{0.8}$, with the spectra of the Se-poorer samples suffering from greater background noise because of the lower Se concentration (Fig. 2b). The remaining *Ch* XPS spectra (Se 3p, Te 4d, Te 3d) are nearly indistinguishable (Fig. S2 in Supplementary Data).

Although BE shifts in the La 3d and Cu 2p spectra cannot be used to extract information about charges, we make the assumption that these atoms are positively charged, with formal oxidation states of La^{3+} and Cu^{+}. The BEs in the O 1s and *Ch* (Se 3d, 3p; Te 4d, 3d) spectra are lower relative to the elements (dashed vertical lines in the spectra) [33], indicating that these atoms are negatively charged. However, the trends in the O 1s and Se 3d BEs with greater substitution *x* in the solid solution $LaCuOSe_{1-x}Te_x$ (Fig. 3a) require different explanations. The decrease in Se 3d BE suggests that the Se atoms, which are more electronegative than Te atoms, must accept a greater burden of the charge transferred in the Cu–*Ch* bonds; each of the diminishing number of Se atoms carries a more negative charge. The occurrence of BE shifts, albeit small, in the O 1s peak is puzzling because the O atoms are not directly bonded to the

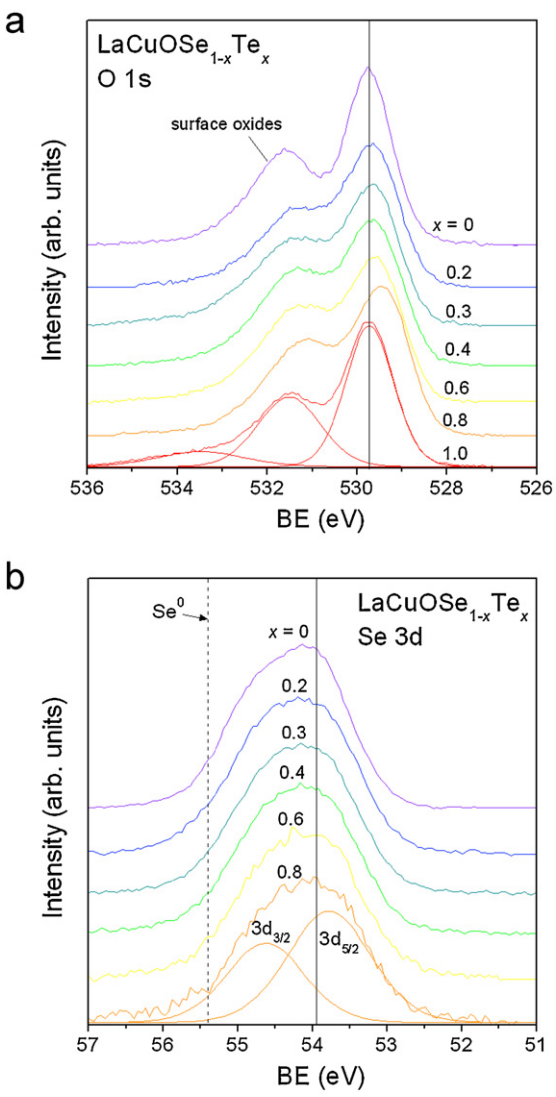

Fig. 2. (a) O 1s and (b) Se 3d XPS spectra for $LaCuOSe_{1-x}Te_x$. The solid vertical lines locate the O 1s and Se $3d_{5/2}$ peaks in LaCuOSe. For reference, the dashed vertical line in (b) marks the Se $3d_{5/2}$ BE in elemental Se.

Ch atoms. However, weak La–*Ch* interactions between the ostensibly independent [LaO] and [Cu*Ch*] layers have been implicated previously [17]. We propose that the O 1s BE shifts are not caused by changes in the charge of the O atoms (an intraatomic effect), but rather by changes in their coordination environment, which modifies the Madelung potential (an interatomic effect). When the charge potential model is applied [34–37], the O 1s BE shifts can be described as:

$$\Delta E_{O1s} = k\Delta q_O + 4\Delta\left(\frac{q_{La}}{d_{O-La}}\right) + 4\Delta\left(\frac{q_O}{d_{O-O}}\right) + 4\Delta\left(\frac{q_{Ch}}{d_{O-Ch}}\right) + \cdots \quad (1)$$

in which the first term represents any inherent changes in the O charge and the subsequent terms represent the contributions of the first, second, and third coordination spheres (CS) around the O atom to the Madelung potential. As more Se is substituted by Te atoms (increasing *x* in $LaCuOSe_{1-x}Te_x$), the La atoms become less positively charged (if the occurrence of La–*Ch* interactions is accepted); that is, the $\Delta(q_{La}/d_{O-La})$ term becomes less positive. Meanwhile, the *Ch* atoms become less negatively charged and more distant (from 3.5 to at 3.7 Å), on average; that is, the $\Delta(q_{Ch}/d_{O-Ch})$ term becomes less negative. Thus, the evolution of these contributions

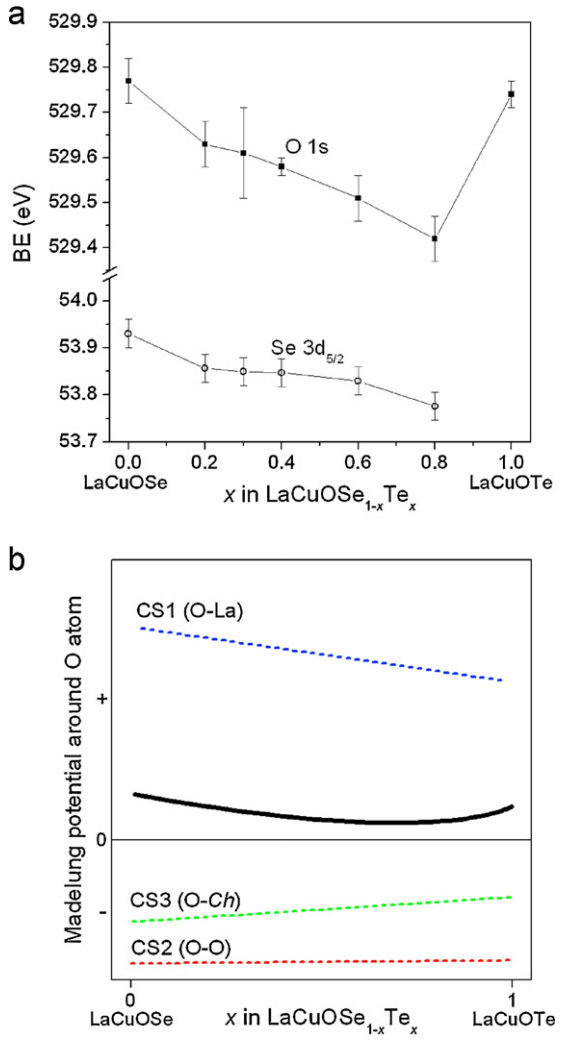

Fig. 3. (a) Plot of O 1s and Se $3d_{5/2}$ BEs vs. x in $LaCuOSe_{1-x}Te_x$. (b) Schematic representation of the contributions (dashed lines) of the first, second, and third coordination spheres (CS) to the Madelung potential (solid line) experienced by the O atom in $LaCuOSe_{1-x}Te_x$.

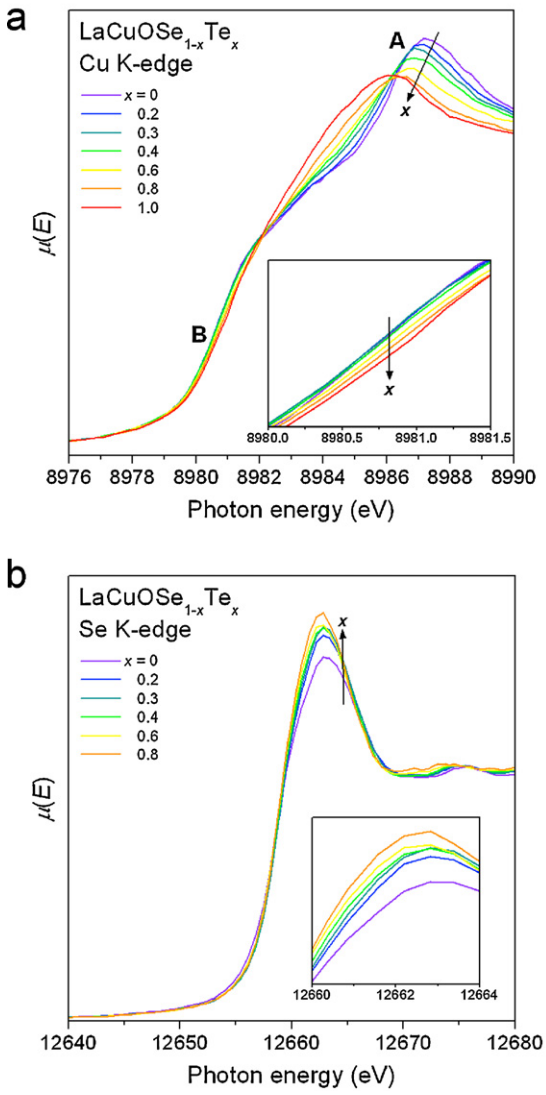

Fig. 4. (a) Cu K-edge and (b) Se K-edge XANES spectra for $LaCuOSe_{1-x}Te_x$.

to the Madelung potential from the first and third CS, respectively, follows opposing trends, as qualitatively shown in Fig. 3b. The summation of these two oppositely sloped lines leads to a minimum in the Madelung potential at some intermediate value of x, as shown by the solid black line in the figure. Because the neighbouring La atoms in the first CS dominate the Madelung potential, the O 1s BE tends to decrease gradually with increasing x. However, at sufficiently high substitution levels, the contribution from the third CS eventually reverses the trend, such that in the end-member LaCuOTe ($x = 1$), the O 1s BE is essentially the same as in LaCuOSe ($x = 0$).

The analysis of the O 1s BE shifts above rests on the assumption that they depend mainly on ground-state effects, but it is worthwhile considering if final-state effects could also account for the observed trends in which the BE is apparently lowered because of interatomic relaxation, as described earlier [32]. Because the immediate environment around each O atom is a tetrahedron of four La atoms, the highly ionic nature of the La–O interactions implies that such relaxation processes are unlikely. However, it is conceivable that as the more distant *Ch* atoms in the third CS become increasingly substituted with less electronegative Te atoms, the La atoms gain more electron density so that this relaxation becomes enhanced. If so, the O 1s BE would decrease monotonically and reach its lowest value at LaCuOTe. As discussed above, the reversal of the trend actually seen at LaCuOTe can be traced to a ground-state effect involving the Madelung potential, implying these final-state effects are less important.

3.2. XANES spectra

Information about the Cu atoms is best extracted through analysis of the Cu K-edge absorption spectra. These spectra are much less influenced by final state effects than the Cu 2p XPS spectra because electrons are excited into bound (or continuum) states, providing partial screening which in turn minimizes relaxation processes. In accordance with the selection rule $\Delta l = \pm 1$, the most prominent feature in the Cu K-edge spectra of $LaCuOSe_{1-x}Te_x$ is assigned to the excitation of Cu 1s electrons to unoccupied 4p states, marked as A in Fig. 4a. This main edge-feature is prominent in other compounds containing tetrahedrally coordinated Cu^{1+} species, such as Cu(I) halides, and is unaffected by multiscattering resonance within the EXAFS region [38]. The absorption-edge energy gradually decreases from 8986.1(1) eV in LaCuOSe to 8985.3(1) eV in LaCuOTe, indicating that the Cu atoms become less positively charged and consistent with diminished Cu-to-*Ch* electron transfer when Se atoms are successively substituted by less electronegative Te atoms. The shift

in the absorption edge to lower energy also agrees with the location of empty Cu-4p-based conduction levels in the density of states for LaCuOSe vs. LaCuOTe (Fig. S3 in Supplementary Data). There is a second, weaker pre-edge feature, marked as B in the spectra, that appears to be fixed in energy (as confirmed by noting the invariance in the maximum of the first derivative in the spectra) but instead becomes slightly less intense on proceeding from LaCuOSe to LaCuOTe. Such a feature is normally assigned as a dipole-forbidden 1s-to-3d transition in Cu^{2+}-containing compounds [39]. Although XPS and Auger spectroscopy indicate that the present compounds contain Cu^{1+} species [17], which have no available empty 3d states, we propose that the transition becomes allowed through mixing of 3d and empty 4p states in the tetrahedrally coordinated Cu atoms (which lack an inversion centre) [16,38]. Cu(I) halides exhibit similar 1s-to-3d/4p pre-edge features, with significant intensity because of the mixing with empty 4p states [38]. The diminished Cu-to-*Ch* charge transfer leads to fewer available empty hybridized 3d/4p-based Cu states to which electrons can be excited and thus lower probability for the absorption process to take place. For comparison at the other extreme, the pre-edge is most intense in LaCuOS (Fig. S4 in Supplementary Data).

The Se K-edge spectra probes transitions from filled Se 1s to empty Se 4p states, as manifested by an absorption edge energy of 12658.2(1)–12658.4(1) eV that is nearly constant, within error, for all members of $LaCuOSe_{1-x}Te_x$ (Fig. 4b). (These spectra are shown in fluorescence mode, providing a smoother background than in the more usually preferred transmission mode, which gave poorer signal-to-noise ratios, especially for samples with low Se concentrations.) Interestingly, the absorption edge signal strengthens in intensity on proceeding from LaCuOSe to $LaCuOSe_{0.2}Te_{0.8}$. This trend runs counter to expectations based on decreasing Se concentration, as has been seen, for instance, in Se K-edge spectra for $FeSe_{1-x}Te_x$, where strong chalcogen–chalcogen bonds (~2.7 Å) are present [40–42]. Although absorption spectra measured in fluorescence mode commonly suffer from self-absorption effects, we consider such effects to be unlikely here because the X-ray energy is quite high (12 keV), which reduces photoionization cross-sections [43], the samples analyzed are thin [44–46], and the Se concentrations are low. Instead, we propose that the La–*Ch* interactions described earlier between the [LaO] and [Cu*Ch*] layers provide a mechanism for hybridization of La- and *Ch*-based conduction states, as confirmed by inspection of the DOS curves in the calculated band structures (Fig. S3 in Supplementary Data). The energy dispersion of these conduction states widens by 0.5 eV on proceeding from LaCuOSe to LaCuOTe, leading to greater probability for absorption from the Se 1s states and thus a more intense absorption edge signal.

4. Conclusions

Further evidence for the occurrence of weak La–*Ch* interactions between the [LaO] and [Cu*Ch*] layers in LaCuO*Ch* has been provided by two major observations. First, the O 1s BEs experience small shifts on proceeding from LaCuOSe to LaCuOTe, not because of inherent changes in the charge of the O atoms, but rather because of changes in the Madelung potential dominated by the diminishing charge of surrounding La atoms as the La–*Ch* interactions strengthen with greater substitution of Se by Te. Second, the trend in the intensity of the Se K-edge can be rationalized through hybridization of La- and *Ch*-based conduction states. Direct evidence for Cu-to-*Ch* charge transfer within the [Cu*Ch*] layers has now also been obtained through the observation of absorption-edge energy shifts and intensity changes in a pre-edge feature in the Cu K-edge spectra, as well as small shifts in the Se 3d BEs. The gradual nature of these BE and absorption edge shifts suggests that the electronic structure can be progressively tuned in these oxychalcogenides.

Acknowledgments

The Natural Sciences and Engineering Research Council (NSERC) of Canada supported this work. Access to the Kratos AXIS 165 XPS spectrometer was provided by the Alberta Centre for Surface Engineering and Science (ACSES), established with support from the Canada Foundation for Innovation and from Alberta Innovation and Science. We thank Dr. Robert Gordon for assistance with the Cu K- and Se K-edge XANES experiments at PNC/XOR-CAT facilities at the APS, with support from the US Department of Energy, NSERC, the University of Washington, and Simon Fraser University.

Appendix A. Supplementary data

Supplementary data associated with this article can be found, in the online version, at doi:10.1016/j.jallcom.2011.11.063.

References

[1] S. Inoue, K. Ueda, H. Hosono, N. Hamada, Phys. Rev. B 64 (2001) 245211-1–245211-5.
[2] K. Ueda, K. Takafuji, H. Hiramatsu, H. Ohta, T. Kamiya, M. Hirano, H. Hosono, Chem. Mater. 15 (2003) 3692–3695.
[3] H. Hiramatsu, H. Kamioka, K. Ueda, M. Hirano, H. Hosono, J. Ceram. Soc. Jpn. 113 (2005) 10–16.
[4] H. Hiramatsu, K. Ueda, H. Ohta, T. Kamiya, M. Hirano, H. Hosono, Appl. Phys. Lett. 87 (2005) 211107-1–211107-3.
[5] K. Ueda, H. Hiramatsu, M. Hirano, T. Kamiya, H. Hosono, Thin Solid Films 496 (2006) 8–15.
[6] H. Hiramatsu, H. Kamioka, K. Ueda, H. Ohta, T. Kamiya, M. Hirano, H. Hosono, Phys. Status Solidi A 203 (2006) 2800–2811.
[7] H. Hiramatsu, H. Yanagi, T. Kamiya, K. Ueda, M. Hirano, H. Hosono, Chem. Mater. 20 (2008) 326–334.
[8] R. Pöttgen, D. Johrendt, Z. Naturforsch. B 63 (2008) 1135–1148.
[9] S.J. Clarke, P. Adamson, S.J.C. Herkelrath, O.J. Rutt, D.R. Parker, M.J. Pitcher, C.F. Smura, Inorg. Chem. 47 (2008) 8473–8486.
[10] B.I. Zimmer, W. Jeitschko, J.H. Albering, R. Glaum, M. Reehuis, J. Alloy Compd. 229 (1995) 238–242.
[11] P. Quebe, L.J. Terbüchte, W. Jeitschko, J. Alloy Compd. 302 (2000) 70–74.
[12] Y. Kamihara, H. Hiramatsu, M. Hirano, R. Kawamura, H. Yanagi, T. Kamiya, H. Hosono, J. Am. Chem. Soc. 128 (2006) 10012–10013.
[13] H. Takahashi, K. Igawa, K. Arii, Y. Kamihara, M. Hirano, H. Hosono, Nature 453 (2008) 376–378.
[14] Y.-W. Ma, Z.-S. Gao, L. Wang, Y.-P. Qi, D.-L. Wang, X.-P. Zhang, Chin. Phys. Lett. 26 (2009) 037401-1–037401-4.
[15] P.E.R. Blanchard, B.R. Slater, R.G. Cavell, A. Mar, A.P. Grosvenor, Solid State Sci. 12 (2010) 50–58.
[16] P.E.R. Blanchard, R.G. Cavell, A. Mar, J. Solid State Chem. 183 (2010) 1477–1483.
[17] B.W. Rudyk, P.E.R. Blanchard, R.G. Cavell, A. Mar, J. Solid State Chem. 184 (2011) 1649–1654.
[18] P.E.R. Blanchard, R.G. Cavell, A. Mar, J. Solid State Chem. 183 (2010) 1536–1544.
[19] A.M. Baergen, P.E.R. Blanchard, S.S. Stoyko, A. Mar, Z. Anorg. Allg. Chem. 637 (2011) 2007–2012.
[20] K. Ueda, H. Hosono, Thin Solid Films 411 (2002) 115–118.
[21] N. Fairley, CasaXPS, Version 2.3.9, Casa Software Ltd., Teighnmouth, Devon, UK, 2003, http://www.casaxps.com.
[22] B. Ravel, M. Newville, J. Synchrotron Radiat. 12 (2005) 537–541.
[23] R. Tank, O. Jepsen, A. Burkhardt, O.K. Andersen, TB-LMTO-ASA Program, Version 4.7, Max Planck Institut für Festkörperforschung, Stuttgart, Germany, 1998.
[24] A.J. Signorelli, R.G. Hayes, Phys. Rev. B 8 (1973) 81–86.
[25] G. Crecelius, G.K. Wertheim, D.N.E. Buchanan, Phys. Rev. B 18 (1978) 6519–6524.
[26] S.-J. Oh, G.-H. Kim, G.A. Sawatzky, H.T. Jonkman, Phys. Rev. B 37 (1988) 6145–6152.
[27] W. Grünert, U. Sauerlandt, R. Schlögl, H.G. Karge, J. Phys. Chem. 97 (1993) 1413–1419.
[28] E. Talik, A. Novosselov, M. Kulpa, A. Pajaczkowska, J. Alloy Compd. 321 (2001) 24–26.
[29] A. Novosselov, E. Talik, A. Pajaczkowska, J. Alloy Compd. 351 (2003) 50–53.
[30] S.K. Chawla, N. Sankarraman, J.H. Payer, J. Electron Spectrosc. Relat. Phenom. 61 (1992) 1–18.
[31] A.C. Miller, G.W. Simmons, Surf. Sci. Spectra 2 (1993) 55–60.
[32] S.W. Gaarenstroom, N. Winograd, J. Chem. Phys. 67 (1977) 3500–3506.
[33] C.D. Wagner, A.V. Naumkin, A. Kraut-Vass, J.W. Allison, C.J. Powell, J.R. Rumble Jr., NIST X-ray Photoelectron Spectroscopy Database, Version 3.5 (web

version), National Institute of Standards and Technology, Gaithersburg, MD, 2003, http://srdata.nist.gov/xps.
[34] A.R. Gerson, T. Bredow, Surf. Interface Anal. 29 (2000) 145–150.
[35] P.A.W. van der Heide, Surf. Sci. 490 (2000) L619–L626.
[36] P.A.W. van der Heide, J. Electron Spectrosc. Relat. Phenom. 151 (2006) 79–91.
[37] A.P. Grosvenor, R.G. Cavell, A. Mar, J. Solid State Chem. 181 (2008) 2549–2558.
[38] T. Chattopadhyay, A.R. Chetal, J. Phys. C: Solid State Phys. 18 (1985) 5373–5378.
[39] J.M. Brown, L. Powers, B. Kincaid, J.A. Larrabee, T.G. Spiro, J. Am. Chem. Soc. 102 (1980) 4210–4216.
[40] B. Joseph, A. Iadecola, L. Simonelli, Y. Mizuguchi, Y. Takano, T. Mizokawa, N.L. Saini, J. Phys.: Condens. Matter 22 (2010) 485702-1–485702-5.
[41] C.L. Chen, C.L. Dong, J.L. Chen, J.-H. Guo, W.L. Yang, C.C. Hsu, K.W. Yeh, T.W. Huang, B.H. Mok, T.S. Chan, J.F. Lee, C.L. Chang, S.M. Rao, M.K. Wu, Phys. Chem. Chem. Phys. 13 (2011) 15666–15672.
[42] C.L. Chen, S.M. Rao, C.L. Dong, J.L. Chen, T.W. Huang, B.H. Mok, M.C. Ling, W.C. Wang, C.L. Chang, T.S. Chan, J.F. Lee, J.-H. Guo, M.K. Wu, Europhys. Lett. 93 (2011) 47003-1–47003-5.
[43] J.H. Scofield, Theoretical Photoionization Cross Sections from 1 to 1500 keV, Lawrence Livermore Laboratory Report, 1973, UCRL-51326.
[44] A. Kisiel, P. Zajdel, P.M. Lee, E. Burattini, W. Giriat, J. Alloy Compd. 286 (1999) 61–65.
[45] L.G. Parratt, C.F. Hempstead, E.L. Jossem, Phys. Rev. 105 (1957) 1228–1232.
[46] E.A. Stern, K. Kim, Phys. Rev. B 23 (1981) 3781–3787.